Selective solid-phase extraction of metal for water decontamination

Sachin Mane, Surendra Ponrathnam, Nayaku Chavan

Polymer Science and Engineering Division, National Chemical Laboratory, Pune 411008, India
Correspondence to: N. Chavan (E-mail: nn.chavan@ncl.res.in)

ABSTRACT: Metal-contaminated industrial effluent is a major concern for human health. Therefore, the removal of metal is of primary importance. In this study, metals were selectively extracted from water. Selective metal recovery was studied with a crown-ether-based polymer, wherein the selectivity was observed for strontium over lead. Parameters influencing the metal recovery, such as the contact time, adsorbent dosage, and metal-ion concentration, were evaluated. Interestingly, the adsorption rate of strontium was exponentially increased for the initial 4 h, and lead was adsorbed exponentially after 6 h. Notably, 98% strontium adsorption and 64% lead adsorption were obtained in 24 h. The Langmuir adsorption isotherm was in good agreement and demonstrated that the reactive sites of the adsorbent were homogeneous with monolayer metal adsorption with an adsorbent. The Freundlich adsorption isotherm was not obeyed by both metals. The pseudo-first-order and pseudo-second-order kinetics indicated that strontium was adsorbed by chemisorption and lead was adsorbed by physisorption. © 2015 Wiley Periodicals, Inc. J. Appl. Polym. Sci. **2016**, *133*, 42849.

INTRODUCTION

Over the last 2 decades, water pollution has been a major concern with regard to human health problems. Industrial wastewater is a major source of pollution because it contains chemicals along with different metals and metal ions. Therefore, their separation from wastewater is essential. Mining, electroplating, tanneries, metallurgical, textile, painting, and car radiator manufacturing activities are major sources[1–4] from which metals originate and contaminate water. Most industrial effluents contain metal-ion concentrations that are much higher than the permissible limit. Nowadays, physicochemical processes, such as chemical precipitation,[5] chemical oxidation or reduction,[6] coagulation–flocculation,[7] reverse osmosis,[8,9] ultrafiltration,[10,11] electrodialysis,[12] flotation,[13,14] ion exchange,[15] membrane separation,[16] filtration,[17] and biological treatment,[18] are used for metal removal. Each method has its own merits and disadvantages. Chemical processes and electrochemical treatments have limitations because these processes work at high metal-ion concentrations only. However, metal recovery with polymer-supported metal-chelating agents has attracted a lot of attention because of its ubiquitous applications in adsorption, and selective separation. It also promises to work at high and low level concentrations of metals in water and is, consequently, preferred industrially. Furthermore, metal ions are nondegradable and highly soluble in water; this allows the mitigation of the concentration of oxygen in water. As a result, drinking water becomes rich in hazardous metals, which accumulate in the human body at larger concentrations than required.

In 1984, the World Health Organization declared[19] that, chromium, copper, zinc, iron, cadmium, and lead are the most hazardous metals that cause poisoning. Metals are not dangerous in their solid state, but when they are converted into their soluble form, metals become hazardous. Strontium and lead are toxic metals that affect the nervous system[20] and produce abnormal behavior and difficulties in learning. Recently, the adsorbent efficiency is a major concern in metal recovery. In most of these cases, metal recovery was studied and found to have a lack of selectivity that attenuated the adsorbent-removal efficiency. In 2014, Huang *et al.*[21] described the applications of magnetic nanoparticles in metal recovery, wherein pure magnetic photocatalysts removed 91.5% of metals; this was followed by 37.4, 19, and 17.6% metal recovery for various nanoparticles. In 2007, Kaminari *et al.*[22] demonstrated metal-recovery efficiencies of 75.8, 89.9, and 30.3% for lead, copper, and nickel, respectively. Indeed, selective metal recovery can be performed with different metal-chelating agents, including calixarene,[23] crown ethers, and cyclodextrin. Crown ether is a well-known selective metal-chelating agent that was previously studied for alkali earth metals.[24] Strontium 87 and lead 207 isotopes are stable metal nuclei and are difficult to disintegrate. Therefore, the removal of strontium and lead from industrial wastewater and their reuse is an essential and economical.

Table I. Monomer–Crosslinker Feed Composition of the Copolymer Synthesized by Suspension Polymerization at Different Crosslink Densities

Crosslinking density (%)	Glycidyl methacrylate		Ethylene dimethacrylate	
	mol	g	mol	g
10	0.1055	14.9918	0.0105	2.090
15	0.0993	14.1145	0.0149	2.9522
20	0.0938	13.3341	0.0188	3.7186
25	0.0889	12.6356	0.0222	4.4048

The reaction conditions were as follows: batch size = 16 mL, AIBN concentration = 2.5 mol%, stirring peed = 500 rpm, reaction time = 3 h, outer phase = H_2O, protective colloid = poly(vinylpyrrolidone), protective colloid concentration = 1 wt %, porogen = 1,2-dichlorobenzene, and porogen concentration = 48 mL (monomer-to-porogen ratio = 1:3 v/v).

Recently, the use of beaded polymers has been an attractive area because of the possibility for reuse and from an economical view. This method is very powerful and effective for metal recovery. Recently, Kacan and Kutahyali[25] used activated carbon for strontium removal. They successfully extracted strontium in the range 14.97–96.54% for 70- and 30-ppm level metal-ion concentration at pH 5 and 50°C. In 2014, Jeyakumar and Chandrasekaran[26] reported the extraction of lead by marine green algae (*Ulva fasciata* carbon). They demonstrated an extraction of lead of more than 90%. In this article, we describes the selective extraction of strontium with polymer-supported dibenzo-18-crown-6-ether (DB18C6) as an adsorbent from a dilute metal-ion solution. In this study, we investigated the effects of the contact time, adsorbent concentration, and metal-ion concentration on the selective metal recovery and examined them in detail. Moreover, the adsorption isotherm and adsorption kinetics were also evaluated.

EXPERIMENTAL

Materials
Ethylene dimethacrylate (98%) and 2,2-dichlorodiethyl ether (99%) were procured from Aldrich. Sodium bicarbonate (>99%) was purchased from SDFCL. Sodium hydroxide (>98%), *n*-butanol, chloroform, strontium chloride hexahydrate (99%), citric acid (99.5%), sodium citrate (99%), acetic acid (99.7%), and arsenazo(III) were procured from Loba Chemie. 2,2′-Azobisisobutyronitrile (AIBN; 98%) was received from AVRA Synthesis Pvt., Ltd. (Hyderabad, India). Poly(vinylpyrrolidone) K90 powder (molecular weight = 360,000 mol/g) and glycidyl methacrylate (>97%) were procured from Fluka. Pyrocatechol (99%), *n*-butanol, lead acetate trihydrate (99%), and 1,2-dichlorobenzene (>98%) were received from Merck, nitric acid was received from Thomas Baker, and tin chloride dihydrate (97%) was received from Qualigens.

Reagent Preparation
A stock solution of strontium chloride hexahydrate and lead acetate trihydrate were prepared with deionized water having a concentration of 100 ppm. Thereafter, working solutions of 5, 10, 15, 20, and 25 ppm were prepared with the stock solution. An arsenazo(III) complexing agent solution (0.05%) was pre-pared by the dissolution of 50 mg of arsenazo(III) in 100 mL of deionized water. Moreover, a 0.1M solution of citric acid and sodium citrate was prepared in deionized water. An acidic buffer of pH 3 was prepared with citric acid and sodium citrate in deionized water.

### Synthesis of Beaded Microspheres
Poly(glycidyl methacrylate-*co*-ethylene dimethacrylate) [poly(-GMA-*co*-EDMA)] was synthesized at four different crosslinking densities by suspension polymerization. The aqueous (continuous) phase was prepared by the dissolution of 1 wt % poly(vinylpyrrolidone) in deionized water, whereas the organic (discontinuous) phase was composed of the monomer (glycidyl methacrylate), crosslinker (ethylene dimethacrylate), initiator (AIBN), and porogen (1,2-dichlorobenzene). The polymer beads were synthesized in a specially designed, double-walled, cylindrical polymerization reactor 11 cm in diameter and 15 cm in height that was equipped with a condenser. The aqueous and organic phases were prepared before polymerization. The organic (continuous) phase was slowly added to a reactor containing the aqueous phase under a stirring speed of 500 rpm. After the complete addition of the organic phase, the temperature was raised to 70°C and maintained for 3 h. The polymers obtained in the form of beads were filtered, washed with water, methanol, and dried at 60°C under reduced pressure. Beaded polymers obtained by suspension polymerization were further purified by the Soxhlet extraction method, wherein methanol was used as an extracting solvent to purify the polymers. The monomer−crosslinker feed compositions are reported in Table I, and the synthesis of poly(GMA-*co*-EDMA) is depicted in Scheme 1.

Synthesis of the Metal-Chelating Agent
The metal-chelating agent was synthesized and included the steps of synthesis of DB18C6 followed by nitration and reduction.

Synthesis of DB18C6. A 1-L, four-necked flask[27] was fitted with a reflux condenser, dropping funnel, thermometer, and nitrogen balloon to maintain an inert atmosphere. The flask was charged with 29.7 g (0.27 mol) of catechol and 180 mL of *n*-butanol. Then, the reaction mixture was stirred for 15 min to dissolve the catechol in *n*-butanol. Subsequently, 10.98 g (0.27 mol) of sodium hydroxide was added, and the resulting mixture was refluxed at 117°C. Furthermore, a solution of 19.98 g (0.14
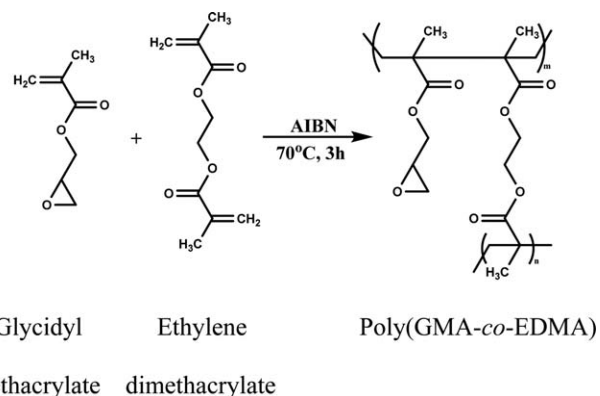
Scheme 1. Synthesis of poly(GMA-*co*-EDMA) by suspension polymerization.
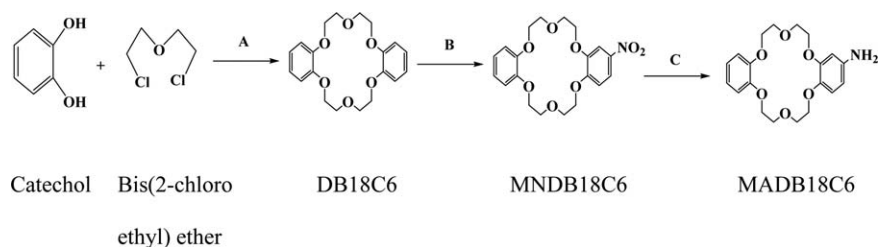
Scheme 2. Synthesis of MADB18C6: (A) NaOH, 117°C, and *n*-butanol; (B) HNO₃, CH₃COOH, chloroform, Δ (61°C), and 2 h; and (C) SnCl₂·2H₂O, HCl, methanol, and reflux.

mol) of bis(2-chloroethyl)ether in 18 mL of *n*-butanol was added dropwise for 2 h under stirring and heating. After complete addition, the reaction mixture was again refluxed for 1 h. Subsequently, the reaction mixture was cooled to 90°C, and 10.98 g (0.27 mol) of sodium hydroxide pellets was again added. Thereafter, the reaction mixture was refluxed for an additional 1 h, and 19.98 g (0.14 mol) of bis(2-chloroethyl)ether in 18 mL of *n*-butanol was added in 2 h. The resulting reaction mixture was refluxed for 16 h. Furthermore, the mixture was acidified with 1.89 mL of hydrochloric acid. Later on, *n*-butanol was distilled out up to 63 mL, and water was added to maintain the same volume. Thus, the resulting slurry was cooled, filtered, and washed with water. Hereinafter, the product was added to 45 mL of acetone and stirred for 5 min. Then, the product was filtered, washed, and dried with suction. Finally, the product was dried at 80°C under reduced pressure to yield 45% DB18C6 polyether (calculated = 48.58 g, experimental = 22 g).

Nitration of DB18C6. A 500-mL round-bottomed flask[28] was fitted with a condenser and nitrogen balloon. The flask was charged with 4.8 g (0.076 mol) of nitric acid, 4.56 g (0.076 mol) of acetic acid, and 160 mL of chloroform and stirred for 5 min. To this, 20 g (0.0555 mol) of DB18C6 was added in 5–6 portions. Subsequently, reaction mixture was stirred for 5 h at room temperature under a nitrogen atmosphere. The completion of reaction was confirmed by TLC. Then, 50% of the chloroform was distilled out. Later, the yellow solid product was filtered and washed with 20 mL of chloroform. Silica gel column was performed to obtain pure mononitrodibenzo-18-crown-6-ether (MNDB18C6) from the mixture of mononitro and dinitro derivatives of DB18C6 with a solvent system of pet ether/ethyl acetate (90:10). The product was dried at 60°C under reduced pressure for 4 h. The yield of MNDB18C6 was 75% (calculated = 22.51 g, experimental = 17 g).

Reduction of MNDB18C6. A 1-L round flask was equipped[29] with a magnetic stirrer, reflux condenser, nitrogen balloon, and thermometer. The flask was charged with 83.48 g (0.37 mol) of SnCl₂·2H₂O, 10 mL (0.274 mol) of hydrochloric acid, and 180 mL of methanol, and the reaction mixture was heated to 65°C to dissolve SnCl₂·2H₂O in methanol. A clear solution of SnCl₂·2H₂O in methanol was obtained after 1 h. Subsequently, 15 g (0.037 mol) of MNDB18C6 was slowly added to solution of SnCl₂·2H₂O. The reaction mixture was stirred and refluxed for 4 h. Later on, 10.97 g (0.274 mol) of sodium hydroxide solution in water was added to the reaction mixture dropwise for 15 min. This mixture was stirred and refluxed for additional 15 min, and reaction completion was confirmed by TLC. The reaction mixture was cooled for 30 min to obtain precipitated solid product. Then, the product was filtered and washed with 15 mL of methanol and dried at 65°C under reduced pressure. A silica gel column was performed to obtain pure monoaminodibenzo-18-crown-6-ether (MADB18C6) from the mixture with a solvent system of pet ether/ethyl acetate (95:5). The yield of the product was 90% (calculated = 13.89 g, experimental = 12.5 g). The synthesis of DB18C6 and their mononitro and monoamino derivatives are represented in Scheme 2.

Synthesis of the Polymer-Supported MADB18C6 as a Selective Chelating Agent

In recent years, polymers are used to potentially support the catalysts, reagents, and metal-chelating agent.[30,31] Poly(GMA-co-EDMA) synthesized by suspension polymerization was modified with DB18C6 for applications in metal chelation from a highly diluted aqueous solution. Polymer modification was carried out in a small reactor with a shaking water bath. An amount of 20 g of polymer was added to a small reactor containing 25 mL of methanol and a catalytic amount of sulfuric acid and stirred at room temperature for 15 min. To this, a MADB18C6 (3 g) solution in 5 mL of methanol was added
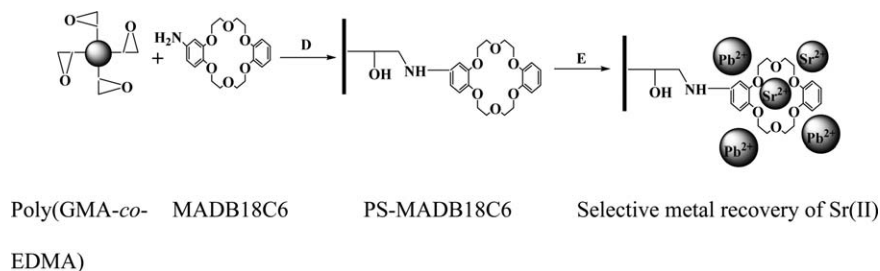
Scheme 3. Synthesis of polymer-supported MADB18C (PS-MADB18C6) and its applications in selective metal recovery: (D) room temperature and H₂SO₄ (catalytic amount) and (E) SrCl₂ and Pb(OAC)₂ solutions in water (ppm).
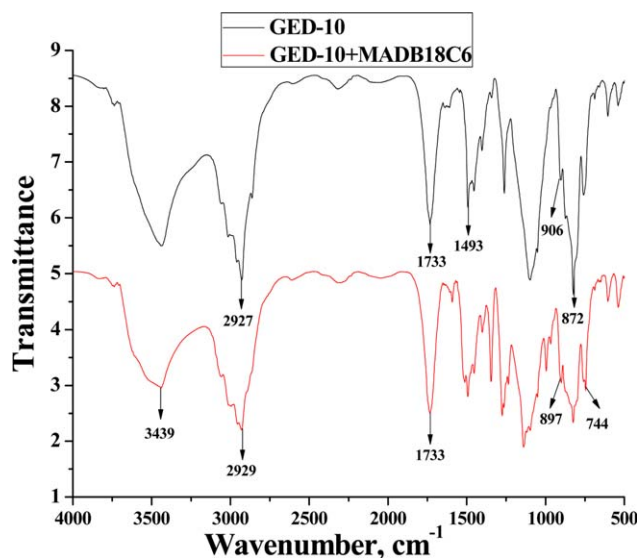
Figure 1. FTIR spectrum of poly(GMA-*co*-EDMA) for 10% CLD (GED-10) and polymer-supported MADB18C6. [Color figure can be viewed in the online issue, which is available at wileyonlinelibrary.com.]

dropwise. Subsequently, reaction mixture was stirred at 60–65°C for 5 h. Then, the modified beaded polymer was filtered and washed with methanol to remove the unreacted crown ether. Later on, the modified polymer was dried at 60−65°C under reduced pressure for 6 h. The synthesis of polymer-supported crown ether is represented in Scheme 3.

Experimental Procedure for the Evaluation of the Effects of the Contact Time, Metal-Ion Concentration, and Adsorbent Dose on Metal Recovery

Effect of the Contact Time. The effect of the contact time was estimated with a 90-ppm metal-ion solution in pH 3 buffer. Polymer-modified DB18C6 (50 mg) was added to a 30-mL capacity glass vial containing 20 mL (90 ppm) of each metal-ion solution. Subsequently, glass vials were placed in a water shaker bath at room temperature. After a certain interval of time, the sample solution was removed for UV spectrometric analysis.

Effect of the Metal-Ion Concentration. The metal-ion concentration effect on the metal recovery was evaluated with polymer-supported DB18C6. A 50 mg of polymer-supported DB18C6 was added to 30-mL-capacity different glass vials containing 20 mL (10, 20, 30, 40, and 50 ppm) of each metal ion in pH 3 buffer solution. Glass vials containing polymer and different metal-ion concentrations were placed in a water shaker bath at room temperature. A sample from each vial was removed after 1 h for UV spectrometric analysis.

Effect of the Adsorbent Concentration. The adsorbent concentration effect was evaluated with 25 ppm of metal-ion solution prepared in buffer having a pH of 3. Furthermore, 20 mL (25 ppm) of a strontium and lead metal solution was added to five different 30-mL-capacity glass vials. To this, different adsorbent concentrations of 30, 60, 90, 120, and 150 mg were added. Subsequently, glass vials were placed in a water shaker bath at room temperature for 2 h. Later on, a sample from each vial was removed to analyze the absorbance with a UV spectrometer. The application of metal-chelating agent in metal recovery is illustrated in Scheme 3.

Characterization

Epoxy-based polymer beads synthesized by suspension polymerization and purified by Soxhlet extractor were used for characterization. The synthesis of polymer beads were confirmed by a Fourier transform infrared (FTIR) spectrometer (KBr, PerkinElmer model Spectrum GX, serial number 69229, number of scans = 10, resolution = 4 cm^{-1}, interval = 1 cm^{-1}). The surface area of the polymer beads was evaluated by the Brunauer–Emmett–Teller method (surface area analyzer, NOVA 2000e, Quantachrome) and particle size distribution was determined by a particle size analyzer (Accusizer 780, model LE 2500-20, PSS.NICOMP particle sizing system, Santa Barbara, CA). Furthermore, the external morphology of the polymer was observed via scanning electron microscopy (SEM; Quanta 200 3D, dual beam Environmental Scanning Electron Microscopy (ESEM) microscope), whereas elemental analysis by microanalysis (Flash EA 1112 series). Metal-chelating agent was synthesized and confirmed by ^{1}H-NMR, ^{13}C-NMR, and FTIR spectroscopy. The synthesis of the polymer-supported metal-chelating agent was
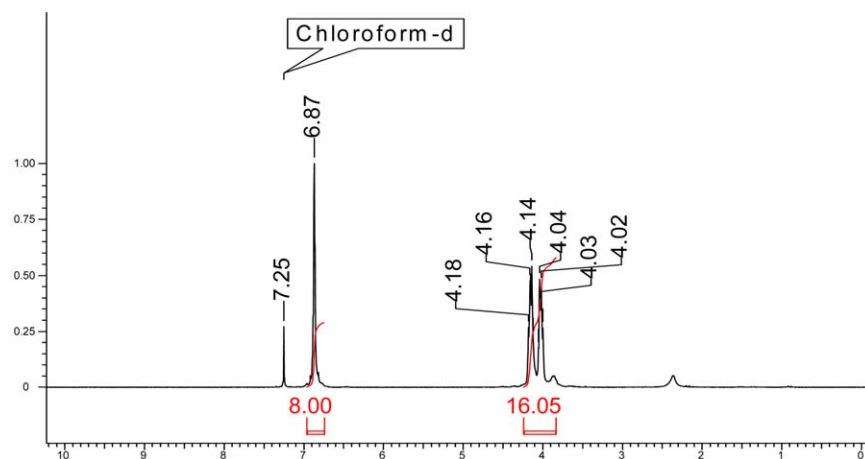
Figure 2. ^{1}H-NMR (200 MHz, CDCl$_3$) of DB18C6. [Color figure can be viewed in the online issue, which is available at wileyonlinelibrary.com.]
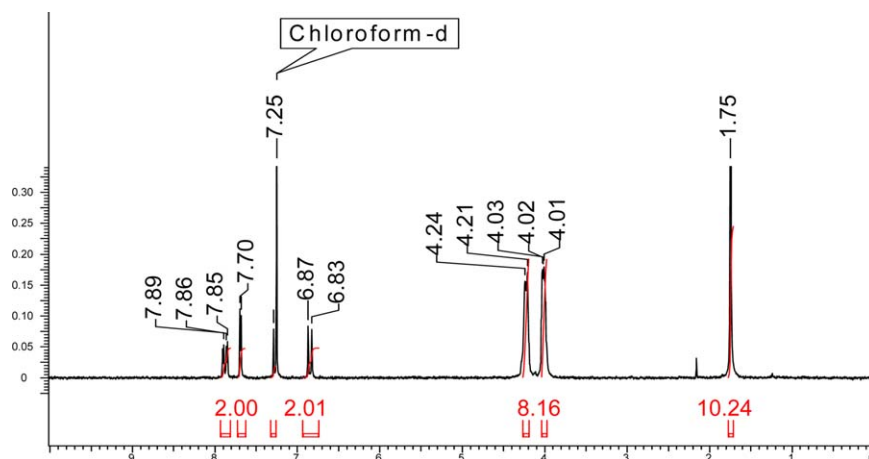
Figure 3. ^{1}H-NMR (200 MHz, CDCl$_3$) of MNDB18C6. [Color figure can be viewed in the online issue, which is available at wileyonlinelibrary.com.]

characterized by surface area determination, particle size analyzer, FTIR spectroscopy (KBr), SEM, and energy-dispersive X-ray (EDX) analysis. The absorbance of the metal complex was measured by an ultraviolet–visible spectrometer (PerkinElmer, Lambda 950).

RESULTS AND DISCUSSION

FTIR Spectroscopy

The synthesis of poly(GMA-co-EDMA) was confirmed by a FTIR (KBr) spectrometer for a 10% crosslinking density.

FTIR spectroscopy (KBr pellets, cm^{-1}): 1733 (—COO—), 906 and 872 (epoxy group),[32] 2927 (aliphatic C—H stretching).

The absorption peak of epoxy (906) vanished after polymer modification with MADB18C6. In addition, peaks at 1733 cm^{-1} (—COO—), 2929 cm^{-1} (aliphatic —C—H stretching), 3439 cm^{-1} (N—H stretching), 1493 cm^{-1} (phenyl ring), 1272 cm^{-1} (C—O stretching), 1048 cm^{-1} (N—H wagging), 897 cm^{-1} (disubstituted phenyl ring), and 744 cm^{-1} (ortho disubstituted phenyl ring) were observed. The FTIR spectrum of poly(GMA-co-EDMA) and polymer-supported DB18C6 are depicted in Figure 1.

^{1}H-NMR, ^{13}C-NMR, FTIR Spectroscopy, and Microanalysis of DB18C6

The synthesis of DB18C6 was confirmed by different techniques, including ^{1}H-NMR, ^{13}C-NMR, FTIR spectroscopy, and elemental analysis.

δ_H (200 MHz, CDCl$_3$): 6.87 (8H, m), 4.02–4.18 (16H, m). δ_C (200 MHz, CDCl$_3$): 148.72, 121.22, 113.39, 69.90, 68.67. FTIR spectroscopy (chloroform, cm^{-1}): 2927 (aliphatic C—H stretching), 1595 (phenyl ring), 1256 (C—O stretching), 1215 (aliphatic ethers), 941 (disubstituted phenyl ring), 756 (ortho disubstituted benzene ring).

ANAL. Found: C, 67.05%; H, 6.69%; O, not determined.

^{1}H-NMR of DB18C6 is shown in Figure 2.

^{1}H-NMR, ^{13}C-NMR, FTIR Spectroscopy, and Microanalysis of MNDB18C6

The synthesis of MNDB18C6 was confirmed by different techniques, including ^{1}H-NMR, ^{13}C-NMR, FTIR spectroscopy, and elemental analysis.
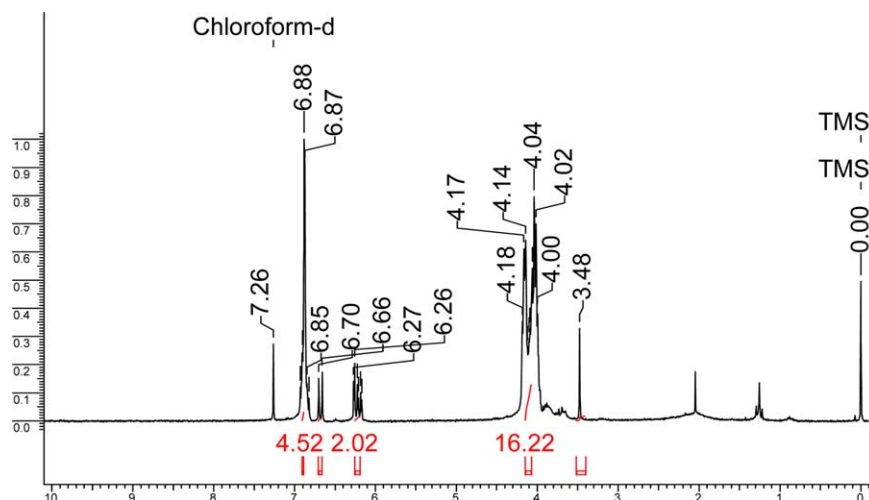
Figure 4. ^{1}H-NMR (200 MHz, CDCl$_3$, Me$_4$Si) of MADB18C6. [Color figure can be viewed in the online issue, which is available at wileyonlinelibrary.com.]
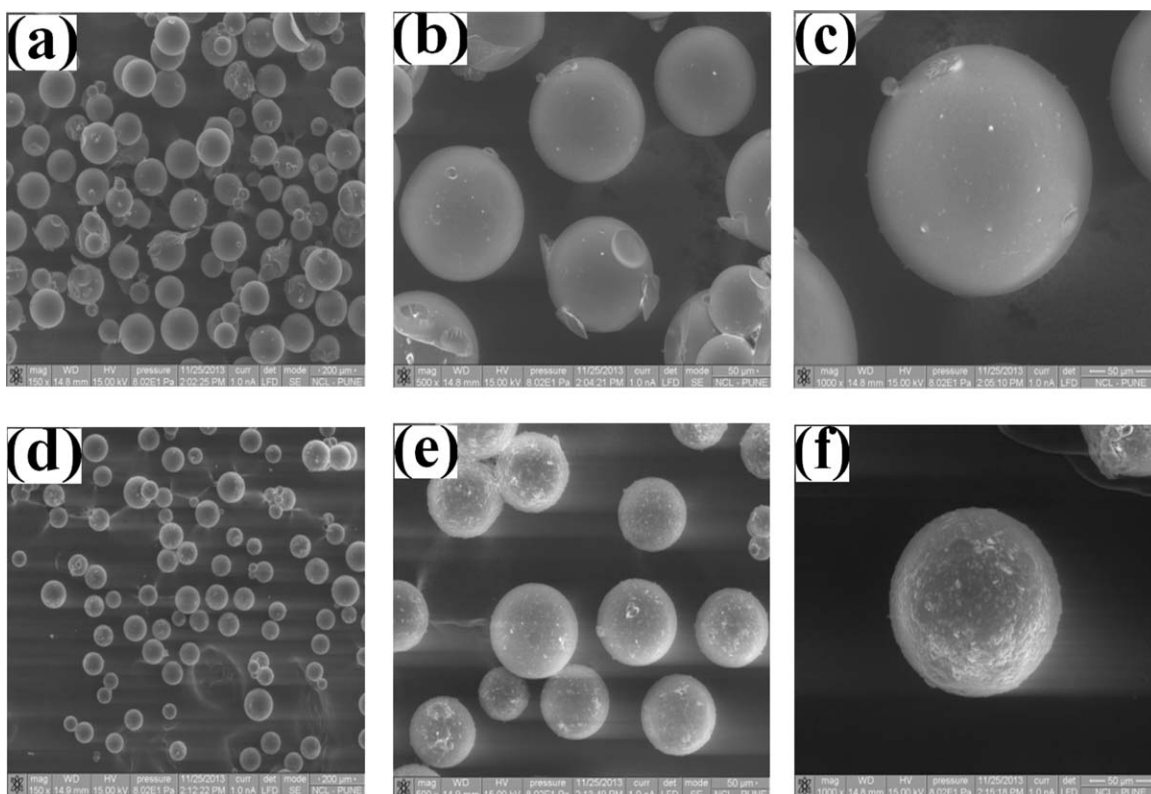
Figure 5. SEM images of (a–c) poly(GMA-*co*-EDMA) and (d–f) polymer-supported DB18C6 (modified) at 150, 500, and 1000× magnifications, respectively.

δ_H (200 MHz, CDCl$_3$): 7.88 (1H, d), 7.69 (1H, S), 6.87 (1H, d), 6.86 (2H, d), 6.84 (2H, dd), 4.03–4.23(16H, m). δ_C (200 MHz, CDCl$_3$): 154.10, 148.71, 144.90, 141.42, 121.25, 117.89, 113.43, 69.87, 69.20. FTIR absorptions (chloroform, cm^{-1}): 3019 (aromatic C—H stretching), 1424 and 1518 (NO$_2$ stretching), 928 (C—N stretching).

ANAL. Found: C, 59.15%; H, 5.56%; N, 2.12%; O, not determined.

^{1}H-NMR of MNDB18C6 is shown in Figure 3.

^{1}H-NMR, ^{13}C-NMR, FTIR Spectroscopy, and Microanalysis of MADB18C6

The synthesis of MADB18C6 was confirmed by different techniques, including ^{1}H-NMR, ^{13}C-NMR, and elemental analysis. δ_H (200 MHz, CDCl$_3$, Me$_4$Si): 6.88 (4H, m), 6.70 (1H, s), 6.22 (2H, d), 4.14 (8H, m), 4.04 (8H, m), 3.48 (2H, s). δ_C (200 MHz, CDCl$_3$): 149.55, 148.60, 141.46, 140.99, 121.03, 115.19, 112.89, 106.82, 101.93, 70.02, 68.45. FTIR spectroscopy(chloroform, cm^{-1}): 3445 (N—H stretching), 1519 (phenyl ring), 1215 (C—O stretching), 1049 (N—H wagging), 929 (disubstituted phenyl ring), 771 (ortho disubstituted benzene ring).

ANAL. Found: C, 52.93%; H, 4.58%; N, 4.92%; O, not determined.

^{1}H-NMR of MADB18C6 is shown in Figure 4.

Surface Area Determination

The surface area is the most important parameter and is attributed to the polymer efficiency. In this study, poly(GMA-*co*-EDMA) was synthesized by suspension polymerization at different crosslinking densities (10, 15, 20, and 25%), and their surface areas were evaluated. Poly(GMA-*co*-EDMA) showed surface areas of 72.76 and 83.11 m^2/g for 10 and 25% crosslinking densities, respectively. On the other hand, polymer-modified crown ether revealed a surface area of 68.76 m^2/g. Obviously, this mitigation in the surface area of polymer was due to the modification with
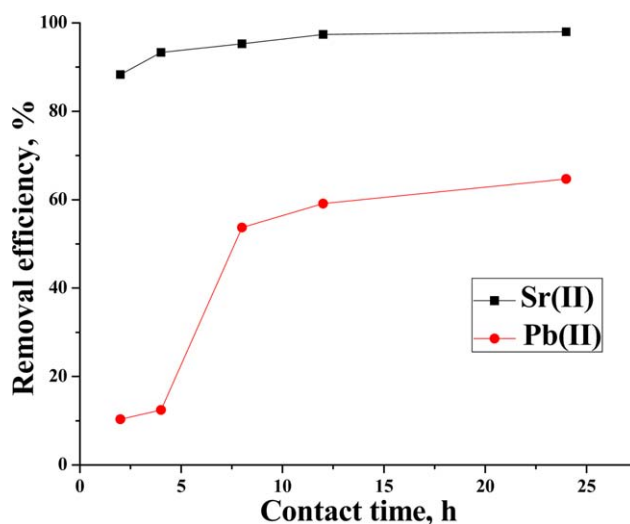
Figure 6. Effect of the contact time on the metal-removal efficiency. [Color figure can be viewed in the online issue, which is available at wileyonlinelibrary.com.]
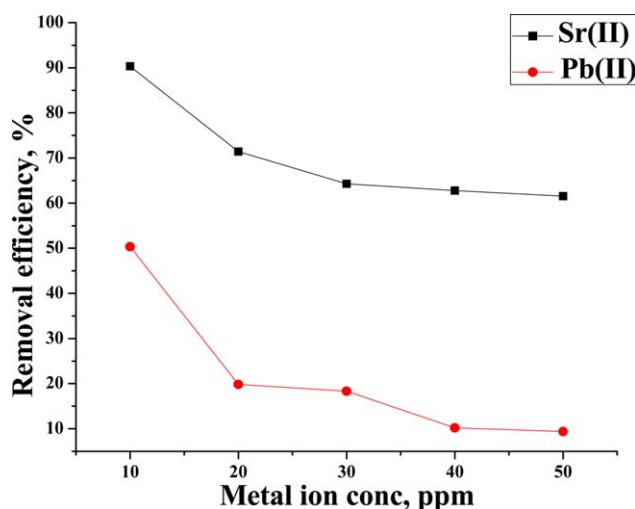
Figure 7. Effect of the metal-ion concentration on the metal-removal efficiency. [Color figure can be viewed in the online issue, which is available at wileyonlinelibrary.com.]

the metal-chelating agent. The high surface area and greater reactivity of the polymer called for a greater loading of the metal-chelating agent (DB18C6) by covalent modification. For the base polymer, the surface area increased with increasing crosslinking density.[33] The surface area of the polymer decreased after modification with DB18C6 because of the loading of the metal-chelating agent.

Particle Size Determination
In recent years, there has been increasing interest in micrometer-sized polymers for various applications. The average particle size of poly(GMA-co-EDMA) was determined at different crosslinking densities. Polymers with crosslinking densities of 10, 15, 20, and 25% demonstrated average particle sizes of 20.32, 24.78, 32.27, and 33.35 μm, respectively. This implied a uniform particle size in the polymer. Nevertheless, the polymer size increased slightly with increasing crosslinking density, and the average particle sizes were in the range 20−34 μm. On the other hand, the polymer-supported MADB18C6 displayed a slightly higher average particle size (32.12 μm) than base polymer. This increased particle size was due to the surface modification of the polymer with DB18C6. This range of average particle sizes was characteristic of suspension polymerization.

SEM: Surface Morphology
SEM image was the visual observation tool that we used to visualize the internal and external surface morphologies. SEM images of the base polymer and polymer modified metal-chelating agent revealed the external morphology and the size of the polymer. SEM images of the unmodified polymer are shown in Figure 5(a–c), whereas those of the polymer-modified DB18C6 are depicted in Figure 5(d–f) with magnifications of 150, 500, and 1000$\times$, respectively. Successful modification was observed because there was a change in the external surface morphology, which could be easily understood from the unmodified and modified SEM images. However, white patches on the surface of the polymer-modified DB18C6 confirmed the modification. Furthermore, a uniform particle size was also one

of the essential pieces of information obtained from the SEM images. Interestingly, the SEM images revealed nonconglomerated beads before and even after modification. SEM images with a 150$\times$ magnification revealed an awesome uniform particle size, whereas those with 500 and 1000$\times$ magnifications displayed the surface morphology of polymers. SEM images of the base and modified polymers with magnifications of 150, 500, and 1000$\times$ are represented in Figure 5.

EDX Analysis
EDX analysis is a powerful tool used for qualitative and quantitative elemental detection. In this study, the base and modified polymers were characterized for elemental detection to confirm polymer modification. EDX analysis revealed that the unmodified polymer contained a carbon concentration of 75.47 wt % (80.39 atom %) and an oxygen concentration of 24.53 wt % (19.61 atom %), whereas the polymer-supported DB18C6 contained a carbon concentration of 62.05 wt % (67.25 atom %), a nitrogen concentration of 16.22 wt % (15.07 atom %), and an oxygen concentration of 21.73 wt % (17.68 atom %). Thus, the absence of nitrogen in the base polymer and its presence in the modified polymer demonstrated successful modification of poly(GMA-co-EDMA).

Selective Metal-Recovery Study by the Spectrometric Method
Metal-ion solutions having concentrations of 5, 10, 15, 20, and 25 ppm were prepared in deionized water, and the absorbances were analyzed for standardization by the spectrometric method. Arsenazo(III) is a complexing agent that forms complexes with a number of metals, including strontium and lead. A complex formed by arsenazo(III) with strontium and lead was analyzed by the spectrometric method. Metal ions had electrostatic interactions[34] with the polymer-supported metal-chelating agent; this encouraged their separation from the aqueous solution.[35]

Effect of the Contact Time. The contact time is a second crucial parameter that substantially influences the metal recovery
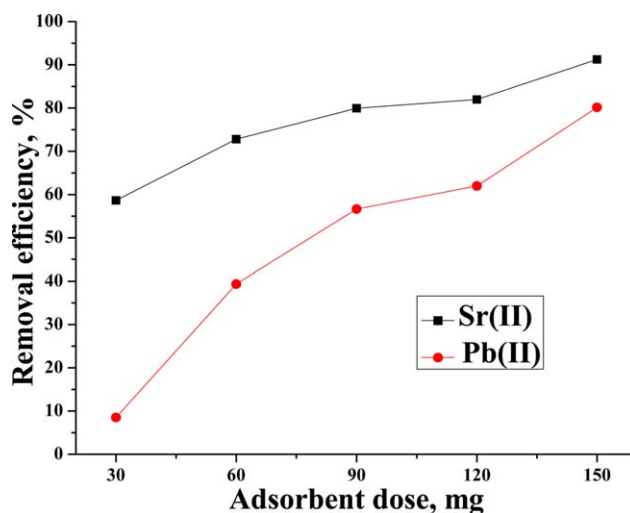
Figure 8. Effect of the adsorbent concentration on the metal-removal efficiency. [Color figure can be viewed in the online issue, which is available at wileyonlinelibrary.com.]
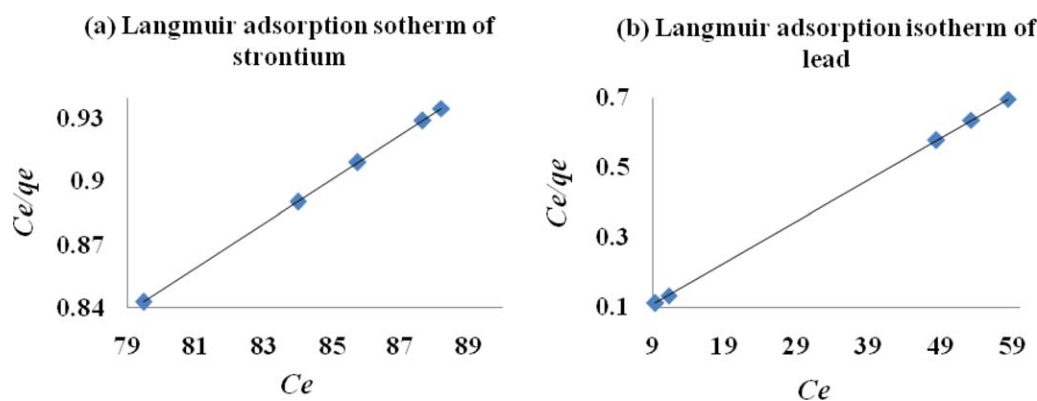
Figure 9. Langmuir adsorption isotherms of (a) strontium and (b) lead. [Color figure can be viewed in the online issue, which is available at wileyonlinelibrary.com.]

(Experimental section). Maximum recoveries of 97.99% strontium and 64.71% lead were obtained. Polymer-supported DB18C6 rendered a higher selectivity for strontium compared to lead at all of the evaluated contact times. Nevertheless, the initial time (4 h) was crucial from the adsorption point of view, mainly because of the exponential adsorption of strontium in the initial 4 h. On the other hand, exponential metal recovery began after 6 h for lead. Perhaps, this was due to the fact that the polymer-supported DB18C6 had a higher electrostatic attraction for strontium over lead. As soon as the concentration of strontium in the metal-ion solution was mitigated, the adsorption rate of lead became exponential after 6 h. The effect of the contact time on the metal-removal efficiency (%) is depicted in Figure 6. To evaluate the maximum recovery, the equilibrium adsorption was analyzed with 20 mL (100 ppm) of a metal-ion solution; this demonstrated that 94.34% Sr(II) and 83.68% lead adsorptions were measured at 24 h.

Effect of the Metal-Ion Concentration. The effect of the metal-ion concentration on the metal recovery was also examined (Experimental section). The results imply that higher metal-ion concentrations attenuated the metal recovery. Furthermore, the maximum recoveries were obtained for a 10-ppm solution; these values were 90.33% strontium and 50.34% lead, whereas 61.56% strontium and 9.40% lead values were obtained for the 50-ppm solution. This was mainly due to the fact that the

adsorbing sites were equal for various metal-ion concentrations. The effects of the metal-ion concentration on the metal-removal efficiency (%) are demonstrated in Figure 7.

Effect of the Adsorbent Dose. In this study, the effect of the adsorbent concentration, which substantially influenced the metal recovery, was evaluated (Experimental section). Indeed, the higher concentration of polymer-supported DB18C6 demonstrated exclusive results compared with the lower adsorbent concentration. However, the lower adsorbent dose revealed an excellent selectivity for strontium over lead. This was mainly due to the fact that the greater concentration of adsorbent contained more adsorptive sites. This ultimately spurred the adsorption of both metals. An inversely small adsorbent concentration had fewer adsorptive sites, and this resulted in the selective recovery of strontium. The effect of the adsorbent dose on the percentage metal-removal efficiency is represented in Figure 8.

Adsorption Isotherm Study. The Langmuir and Freundlich adsorption isotherms of Sr(II) and Pb(II) were investigated at pH 3 and room temperature for certain intervals of time. The Langmuir and Freundlich adsorption isotherms were applied to estimate the selective adsorption capacities of Sr(II) and Pb(II) with polymer-supported DB18C6. However, the adsorption study was well-fitted by the least-squares method to linearly
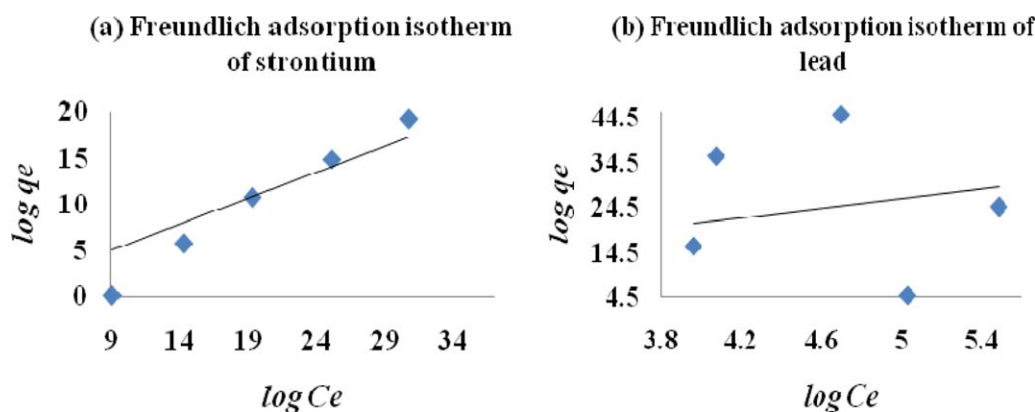
Figure 10. Freundlich adsorption isotherms of (a) strontium and (b) lead. [Color figure can be viewed in the online issue, which is available at wileyonlinelibrary.com.]
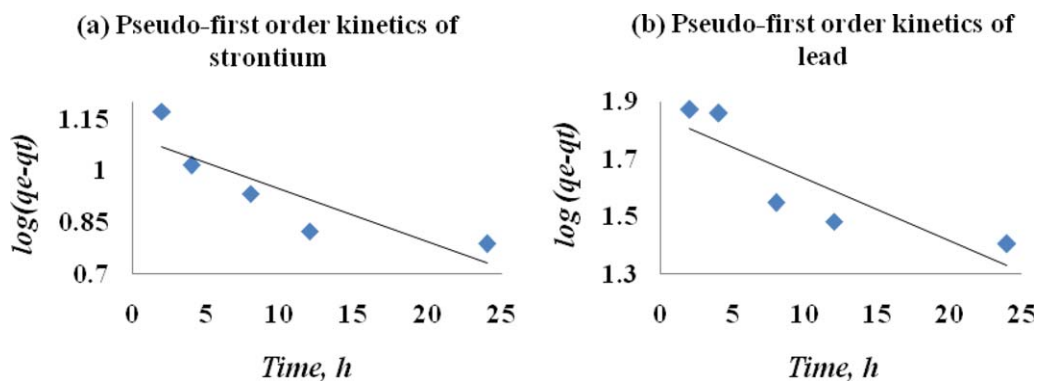
Figure 11. Pseudo-first-order kinetics of (a) strontium and (b) lead. [Color figure can be viewed in the online issue, which is available at wileyonline-library.com.]

transform the Langmuir adsorption isotherm. The linear Lang-muir adsorption isotherm[34,35] is shown by (1):

$$\frac{C_e}{q_e} = \frac{1}{Q_0 b} + \frac{C_e}{Q_0} \qquad (1)$$

where C_e is the equilibrium concentration (mg/L), q_e is the amount of metal adsorbed per gram at equilibrium (mg/g), and Q_0 and b are the Langmuir constants associated with the adsorption capacity (mg/L) and energy of adsorption, respectively.

Figure 9 shows that the adsorption isotherms of strontium and lead fit well with the linear Langmuir adsorption isotherm; this indicated that the reactive sites of an adsorbent were homogeneous, and metal adsorption occurred in a monolayer. The Langmuir adsorption isotherm (C_e/q_e vs C_e) is depicted in Figure 9.

The Freundlich adsorption isotherm was also studied to confirm the possibility of the bilayer adsorption of strontium and lead metals with polymer-supported DB18C6. The linear Freundlich adsorption isotherm[36,37] is shown by (2):

$$\log q_e = \log K_f + \frac{1}{n} \log C_e \qquad (2)$$

where K_f is the adsorption capacity constant and $1/n$ is the measure of adsorption intensity.

The Freundlich adsorption isotherm is nonlinear and was not obeyed by both metals. Thus, the Langmuir and Freundlich adsorption isotherms indicated that the reactive sites of an adsorbent were homogeneous and obeyed monolayer adsorption and not bilayer adsorption. The Freundlich adsorption isotherm of both strontium and lead is illustrated in Figure 10.

Pseudo-First-Order and Pseudo-Second-Order Kinetics. In most cases, kinetic models are used to evaluate the metal adsorption rate and the adsorption mechanism. In this study, pseudo-first-order and pseudo-second-order kinetic models were investigated to evaluate the sorption dynamics of Sr(II) and Pb(II). Kinetic and equilibrium adsorptions are two important physico-chemical parameters. The kinetic adsorption describes the relationship between the contact time and metal adsorption rate, whereas the equilibrium adsorption describes the distribution of metal between the solid and liquid phases, which determines the feasibility and capacity of the metal for adsorption. Nowadays, a number of models are available to explain the adsorption mechanism. The widely used kinetic model is the pseudo-first-order Lagergren[38,39] kinetic equation (3):

$$\log (q_e - q_t) = \log q_e - \frac{K_{ad} t}{2.303} \qquad (3)$$

where q_t is the mass of metal adsorbed at time t (mg g^{-1}), K_{ad} is the pseudo-first-order kinetics constant (L h^{-1}), and t is the time (h).
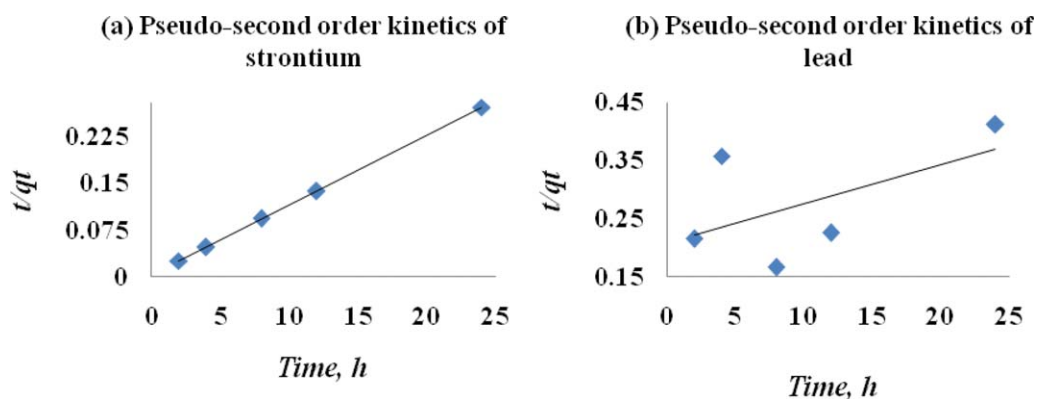
Figure 12. Pseudo-second-order kinetics of (a) strontium and (b) lead. [Color figure can be viewed in the online issue, which is available at wileyonline-library.com.]

Furthermore, pseudo-first-order kinetics determine the rate of occupation of adsorption sites. The plot of $\log(q_e - q_t)$ versus t revealed a straight line, which indicated the application of the pseudo-first-order kinetic model. The plot of $\log(q_e - q_t)$ versus t of strontium and lead are depicted in Figure 11(a,b).

In pseudo-second-order kinetics, physicochemical interactions between the polymer-supported DB18C6 and metals in an aqueous medium were attributed to metal removal. The pseudo-second-order kinetics plot (t/q_t versus t) of the equilibrium adsorption capacity of strontium carried out at room temperature is shown in Figure 12(a). Moreover, the equilibrium adsorption plot of lead is represented in Figure 12(b). Most importantly, this observation clearly demonstrates that strontium obeyed chemisorption, whereas lead did not obey chemisorption. Thus, pseudo-first-order and pseudo-second-order kinetics revealed that strontium was adsorbed by chemisorption, and lead adsorbed by physisorption. The pseudo-second-order kinetic equation was applied to this study to determine the equilibrium adsorption[39,40] of the polymer-supported DB18C6 with (4):

$$\frac{t}{q_t} = \frac{1}{K_{2ad} q_e^2} + \frac{t}{q_e} \tag{4}$$

where K_{2ad} is the second-order kinetics rate equilibrium constant (g mg^{-1} min^{-1}).

CONCLUSIONS

In conclusion, polymer-supported DB18C6 displayed a higher selectivity for strontium over lead in an aqueous medium. It is worth noting that 98% strontium and 64% lead adsorptions were obtained in 24 h. Remarkably, an inspection of the contact time data revealed that the initial 4 h was the exponential adsorption period of strontium, whereas the exponential adsorption of led began after 6 h. Notably, a higher selectivity was observed for strontium than for lead during the initial 4 h. In addition, an increasing adsorbent concentration and attenuation in the metal-ion concentration demonstrated a higher metal recovery. The Langmuir adsorption isotherm fit well with both metals in contrast to the Freundlich adsorption isotherm, which was not obeyed. We concluded that the adsorption reactive sites were homogeneous, whereas strontium and lead formed monolayer and bilayer adsorptions, respectively, with the polymer-supported DB18C6. Moreover, strontium and lead were adsorbed by chemisorption and physisorption, respectively.

ACKNOWLEDGMENTS

REFERENCES

1. Turhanen, P. A.; Vepsalainen, J. J.; Peraniemi, S. *Sci. Rep.* **2015**, *5*, 8992.

2. Yen, H. Y.; Kang, S. F.; Lin, C. P. *Water* **2015**, *87*, 312.

3. Laniyan, T. A.; Kehinde Phillips, O. O.; Elesha, L. *Int. J. Eng. Technol.* **2011**, *11*, 61.

4. Kadirvelu, K.; Thamaraiselvi, K.; Namasivayam, C. *Bioresour. Technol.* **2001**, *76*, 63.

5. Chen, Q.; Luo, Z.; Hills, C.; Xue, G.; Tyrer, M. *Water Res.* **2009**, *43*, 2605.

6. Chen, X.; Huang, G.; Wang, J. *J. Metall. Eng.* **2013**, *2*, 161.

7. Semerjian, L.; Ayoub, G. M. *Adv. Environ. Res.* **2003**, *7*, 389.

8. Bakalar, T.; Bugel, M. *Gajdosoya. Acta Montanistica Slovaca Rocnik* **2009**, *14*, 250.

9. Sastri, V. S. *Sep. Sci. Technol.* **1978**, *13*, 541.

10. Vieira, M.; Tavaresa, C. R.; Bergamasco, R.; Petrus, J. C. C. *J. Membr. Sci.* **2001**, *194*, 273.

11. Borbelly, G.; Nagy, E. *Hung. J. Ind. Chem.* **2008**, *36*, 17.

12. Moura, R. C. A.; Bertuol, D. A.; Ferreira, F. A.; Amado, F. D. R. *Int. J. Chem. Eng.* **2012**, *2012*, 1.

13. Zouboulis, A. I.; Matis, K. A. *Water Sci. Technol.* **1995**, *31*, 315.

14. Salmani, M. H.; Davoodi, M.; Hassan, M.; Ghaneian, E. H. T.; Fallahzadah, M. H. *Iran. J. Environ. Health Sci. Eng.* **2013**, *10*, 1.

15. Erdem, E.; Karapinar, N.; Donat, R. *J. Colloid Interface Sci.* **2004**, *280*, 309.

16. Alaguraj, M.; Palanivelu, K.; Velan, M. *Int. J. Chem. Tech. Res.* **2009**, *1*, 722.

17. Barakat, M. A. *Arabian J. Chem.* **2011**, *4*, 361.

18. Vasquez, T. G. P.; Botero, A. C. E.; De Mesquita, L. M. S.; Torem, M. L. *Miner. Eng.* **2007**, *20*, 939.

19. Shahmohammadi-Kalalagh, S.; Babazadeh, H.; Nazemi, A. H.; Manshouri, M. *Caspian J. Environ. Sci.* **2011**, *9*, 243.

20. Needleman, H. L.; Bellinger, D. *Arch. Clin. Neuropsychol.* **2001**, *16*, 359.

21. Huang, S.; Gu, L.; Zhu, N.; Feng, K.; Yuan, H.; Lou, Z.; Li, Y.; Shan, A. *Green Chem.* **2014**, *16*, 2696.

22. Kaminari, N. M. S.; Schultz, D. R.; Ponte, M. J. J. S.; Ponte, H. A.; Marino, C. E. B.; Neto, A. C. *Chem. Eng. J.* **2007**, *126*, 139.

23. Chen, X.; Ji, M.; Fisher, D. R.; Wai, C. M. *Inorg. Chem.* **2009**, *38*, 5449.

24. Choi, C. M.; Heo, J.; Kim, N. *J. Chem. Cent. J.* **2012**, *6*, 84.

25. Kacan, E.; Kutahyali, C. *J. Anal. Appl. Pyrolysis* **2012**, *97*, 149.

26. Jayekumar, R. P. S.; Chandrasekaran, V. *Int. J. Ind. Chem.* **2014**, *5*, 1.

27. Pedersen, C. *J. Org. Synth.* **1988**, *6*, 395.

28. Klyatskaya, S. V.; Tretyakov, E. V.; Vasilevsky, S. F. *Arkivoc* **2003**, *13*, 21.

29. Racane, L.; Stojkovic, R.; Tralic-Kulenovic, V.; Karminski-Zamola, G. *Molecules* **2006**, *11*, 325.

30. Shunmughanathan, M.; Puthiaraj, P.; Pitchumani, K. *ChemCatChem* **2015**, *7*, 666.

31. Iemma, F.; Cirillo, U. G.; Spizzirri, G.; Puoci, F.; Parisi, O. I.; Picci, N. *Eur. Polym. J.* **2008**, *44*, 1183.

32. Theophanides, T.; Velasco-Santos, C.; Martinez-Hernandez, A. L. *Mater. Sci. Eng. Technol.* **2012**, *13*, 261.

33. Rahman, A. U.; Iqbal, M.; Rahman, F. U.; Dayan, F. D.; Yaseen, M. L.; Omer, M.; Garver, M.; Yang, L.; Tan, T. *J. Appl. Polym. Sci.* **2012**, *124*, 915.

34. Eley, M. D. Ph.D. Thesis, Texas Tech University, **1996**.

35. Lo, S. F.; Wang, S. Y.; Tsai, M. J.; Lin, L. D. *Chem. Eng. Res. Des.* **2012**, *90*, 1397.

36. Mittal, A.; Kurup, L.; Mittal, J. *J. Hazard. Mater.* **2007**, *146*, 243.

37. Okeola, F. O.; Odebunmi, E. O. *Adv. Nat. Appl. Sci.* **2010**, *4*, 281.

38. Robati, D. *J. Nanostruct. Chem.* **2013**, *3*, 1.

39. Ho, Y. S.; McKay, G. *Process Biochem.* **1999**, *34*, 451.

40. Ho, Y. S. *Scientometrics* **2004**, *59*, 171.